

Particle-wall collision statistics in the open circular billiard

Jürgen F. Stilck*

Instituto de Física

Universidade Federal Fluminense

Av. Litorânea s/n

24210-346 - Niterói, RJ

Brazil

(Dated: December 2, 2024)

We study the problem of the open circular billiard (particles inside a circular vesicle with specular collisions at the wall, escaping through an aperture described by an angle 2δ), considering the distributions of probability at successive times n the particle reaches the border of the vesicle. These distributions are calculated analytically and measured in numerical simulations. The selection of angular momenta close to periodic orbits which never escape from the vesicle is observed after some collisions. In general, we calculate the marginal distributions up to $n = 4$, but for $\delta > \pi/2$ a solution is found for arbitrary n . The escape probability as a function of n^{-1} decays with an exponent 4 for $\delta > \pi/2$ and evidences for a power law decay are found for lower apertures as well.

PACS numbers: 45.50.-j, 05.20.-y, 02.70.-c

I. INTRODUCTION

In the theory of dynamical systems, the study of the decay of simple hamiltonian systems [1, 4, 5] is of much interest. These studies are an extension of earlier research concerning the closed version of such systems, where the main question is their ergodicity. The pioneering work in this area is centered on the system called Sinai billiard, a circular billiard with a smaller circular exclusion area in its interior [6], which was shown to be ergodic. Other two-dimensional ballistic billiards are known to be ergodic as well, such as the Bunimowitch stadium [4, 7]. One main interest in the studies of open billiards is the decay dynamics for long times. Bauer and Bertsch [1] found an exponential decay in an chaotic dynamics and a power law decay for a system with regular dynamics. These first results concerning the integrable case where later questioned by Legrand and Sornette [2], but it became clear that the difficulty in settling this question using numerical experiments is related to the high sensitivity of the results to initial conditions [3]. In a more detailed simulational study for the chaotic two-dimensional Bunimovich stadium [4], algebraic tails were found at sufficiently long times, but the algebraic decay vanishes in the limit of zero hole size.

In the classical circular billiard the (non-interacting) particles undergo elastic specular collisions with the wall. Since two quantities are conserved (kinetic energy and angular momentum), the system is integrable and therefore non-ergodic [8]. A recent study of the open version of this system was undertaken by Vicentini and Kokshenev [5], and the algebraic long time of the survival probability was studied in detail, in the limit of a very small opening (*weakly open billiard*), using a coarse-grained description

of the system. Here we study the problem making use of a probabilistic approach: starting from a random initial condition of the particles inside the vesicle, we calculate the joint probability distribution at successive times the border of the vesicle is reached. This approach is not limited to small openings, actually it allows a full analytical treatment when the opening δ is larger than $\pi/2$ ($\delta = \pi/2$ corresponds to a semi-circular vesicle). It will become clear below that for higher number of collisions with the wall, those particles which are close to periodic orbits which will never leave the vesicle will still survive, and thus a selection of these orbits will occur with increasing number of collision n . This selection of orbits according to the incidence angle (or, equivalently, to the angular momentum) was already found in the numerical experiments performed in [5], and emerges in a simple way in the probabilistic calculations below. The algebraic decay of the probability that the particle leaves the vesicle at the n 'th collision is obtained analytically for large openings ($\delta > \pi/2$).

Let us define the problem. The initial position of a particle is distributed uniformly inside the circular vesicle of radius r_0 . The particle has a velocity of modulus v_0 , whose direction is also uniformly distributed. After some time, this particle reaches the border of the vesicle for the first time, at an angle θ_1 . If $|\theta_1| < \delta$, the opening angle, the particle leaves the vesicle, otherwise it collides with the wall and performs the second straight part of its movement inside the billiard. If we use r_0 as our unit of length and r_0/v_0 as our unit of time we may reduce the problem to the case of unitary radius and modulus of velocity.

In Sec. II we define the problem in more detail and present the analytical approach we adopted. The numerical study of the problem is described in Sec. III, and the simulational results are compared with the analytical ones and discussed. Further discussions and the conclusion may be found in Sec. IV.

*Electronic address: jstilck@if.uff.br

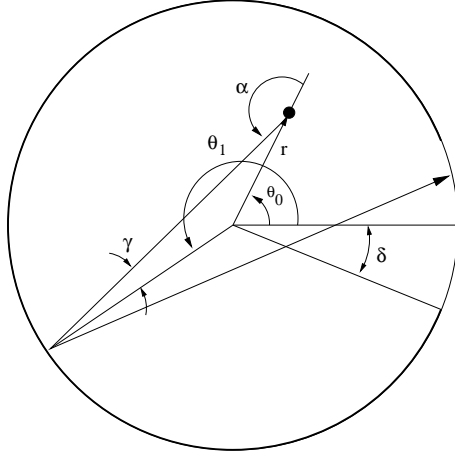


FIG. 1: Movement of a particle, depicted at its initial position. This particle leaves the vesicle when it reaches the border for the second time

II. DEFINITION OF THE PROBLEM AND ANALYTICAL APPROACH

As discussed in Sec. I, we consider a particle inside a circular vesicle of unitary radius. The probability of the initial position, described by a radius r ($0 \leq r \leq 1$) and an angle θ_0 ($-\pi \leq \theta_0 < \pi$), is uniformly distributed. The modulus of the initial velocity is unitary and the angle α ($-\pi \leq \alpha < \pi$) between the position vector and the velocity is also uniformly distributed. Somewhat later, the particle reaches the border of the vesicle for the first time. If the angle θ_1 where this occurs is such that $-\delta \leq \theta_1 \leq \delta$, the particle leaves the vesicle. Otherwise, the particle collides in a specular way with the border of the vesicle, continuing its movement until the border is reached for a second time at an angle θ_2 . In figure 1 the trajectory of a particle is illustrated.

The movement of the particle is deterministic, but the initial conditions are randomly distributed, and we are interested in the joint distribution of probabilities at the n 'th time the border is reached. The initial joint distribution function is given by:

$$\rho_0(r, \alpha, \theta_0) = \frac{r}{2\pi^2}, \quad (1)$$

and this leads to the marginal distributions $\rho_0(r) = 2r$ and $\rho_0(\alpha) = \rho_0(\theta) = 1/2\pi$, which are consistent with the initial conditions stated above. Simple geometrical considerations allow us now to relate the variables γ_1 and t_1 and θ_1 at the first time the particle reaches the border with the original variables r , α , and θ_0 . Notice that t_1 , the time of the first arrival at the border, is numerically equal to the distance between the initial position and the position of first arrival at the border. The angle of incidence γ_1 is defined in the interval $-\pi/2 \leq \gamma_1 \leq \pi/2$, and negative values correspond to particles moving clockwise in the vesicle. With this convention, the signs of α

and γ are the same. The relations between the variables may be found applying trigonometric considerations to the initial segment of the trajectory illustrated in figure 1. The result is:

$$r = \sqrt{t_1^2 - 2t_1 \cos(\gamma_1) + 1} \quad (2a)$$

$$\tan(\alpha) = \frac{\sin(\gamma_1)}{\cos(\gamma_1) - t_1} \quad (2b)$$

$$\theta_0 = \theta_1 + \alpha - \gamma_1 \quad (2c)$$

The joint distribution at the first arrival at the border is related to the initial joint distribution as follows:

$$\rho_1(\gamma_1, t_1, \theta_1) = \rho_0(r, \alpha, \theta_0) \left| \frac{\partial(r, \alpha, \theta_0)}{\partial(\gamma_1, t_1, \theta_1)} \right|. \quad (3)$$

The jacobian may then be calculated using expressions 2. The result is:

$$|J| = \frac{\cos(\gamma_1)}{\sqrt{t_1^2 - 2t_1 \cos(\gamma_1) + 1}}, \quad (4)$$

and using the initial distribution 1, we obtain the joint distribution at the first arrival at the border

$$\rho_1(\gamma_1, t_1, \theta_1) = \frac{\cos(\gamma_1)}{2\pi^2}. \quad (5)$$

From the joint distribution 5 the marginal distributions may then be calculated. The result for t_1 is:

$$\begin{aligned} \rho_1(t_1) &= \frac{1}{2\pi^2} \int_{-\pi}^{\pi} d\theta_1 \int_{-\arccos(t_1/2)}^{\arccos(t_1/2)} \cos(\gamma_1) d\gamma_1 \\ &= \frac{2}{\pi} \sqrt{1 - t_1^2/4} \end{aligned} \quad (6)$$

and the marginal distributions of the other two variables follow in a similar way:

$$\rho_1(\gamma_1) = \frac{2}{\pi} \cos^2(\gamma_1), \quad (7)$$

$$\rho_1(\theta_1) = \frac{1}{2\pi}. \quad (8)$$

As expected, the distribution of θ_1 is uniform. The probability that the particle leaves the vesicle at the first arrival at the border is given by:

$$p_1 = \int_{-\delta}^{\delta} \rho_1(\theta_1) \, d\theta_1 = \frac{\delta}{\pi}. \quad (9)$$

Due to angular momentum conservation, the incidence angle will be the same at each subsequent time the particle reaches the border. Also, the time interval between the first and n 'th times at the border will simply be $t'_n = t_n - t_1 = 2(n-1)\cos(\gamma)$. We therefore consider this interval in the subsequent collisions and reduce our parameter space to the variables γ_n and θ_n . Integrating $\rho_1(t_1, \gamma_1, \theta_1)$ over t_1 , we will get:

$$\rho_1(\gamma_1, \theta_1) = \frac{1}{\pi^2} \cos^2(\gamma_1). \quad (10)$$

Now we may relate the variables at the first and second times the border is reached:

$$\gamma_1 = \gamma_2, \quad (11a)$$

$$\theta_1 = \theta_2 - \pi + 2\gamma_2. \quad (11b)$$

The jacobian of this transformation is unitary, and thus the joint distribution at the second time the border is reached will be

$$\rho_2(\gamma_2, \theta_2) = \frac{\cos^2(\gamma_2)}{\pi^2} f(\theta_1, \delta), \quad (12)$$

where the function $f(\theta_1, \delta) = 1$ if $|\theta_1| > \delta$, and vanishes otherwise, so that only particles which did not leave the vesicle at the first time the border was reached do contribute. Actually θ_1 in the right hand side of equation 12 should be written as a function of θ_2 and γ_2 using the equations 11. It is now easy to generalize this result for the n 'th time the particle reaches the border:

$$\rho_n(\gamma_n, \theta_n) = \frac{\cos^2(\gamma_n)}{\pi^2} \prod_{i=1}^{n-1} f(\theta_i, \delta). \quad (13)$$

We remark that in the absence of the aperture, the joint distribution will be the same at any collision.

Next, we may calculate the marginal distributions at the second time the particle reaches the border. The results are

$$\begin{aligned} \rho_2(\gamma_2) &= \frac{\cos^2(\gamma_2)}{\pi^2} \int_{-\pi}^{\pi} f(\theta_2 - \pi + 2\gamma_2, \delta) d\theta_2 \\ &= \frac{2}{\pi^2} (\pi - \delta) \cos^2(\gamma_2), \end{aligned} \quad (14)$$

and

$$\rho_2(\theta_2) = \frac{1}{2\pi^2} [\pi - \delta + \cos(\theta_2) \sin(\delta)]. \quad (15)$$

One notices that the distribution in θ_2 is no longer uniform if $\delta > 0$, displaying a maximum at $\theta_2 = 0$. This may be explained qualitatively by the effect that due to the aperture, it will be more probable for a particle to have a positive than a negative horizontal component of the velocity after the first collision, since all particles which left the vesicle would have negative horizontal components if they had collided with the wall. Also, comparing the marginal distributions $\rho_1(\gamma_1)$ and $\rho_2(\gamma_2)$, we notice that they differ just by a factor $1 - \delta/\pi$, which accounts for the particles that left the vesicle at the first time the border was reached. The distribution of t'_2 may be obtained from $\rho_2(\gamma_2)$:

$$\begin{aligned} \rho_2(t'_2) &= 2\rho_2(\gamma_2) \left| \frac{d\gamma_2}{dt'_2} \right| \\ &= \frac{2\tau_2^2(\pi - \delta)}{\pi^2 \sqrt{1 - \tau_2^2}}, \end{aligned} \quad (16)$$

where we defined $\tau_2 = t'_2/2$, which is restricted to the interval $[0, 2]$. The probability that the particle leaves

the vesicle at the second time it reaches the border will be:

$$\begin{aligned} p_2 &= 2 \int_0^\delta \rho_2(\theta_2) d\theta_2 = \\ &= \frac{1}{\pi^2} [\delta(\pi - \delta) + \sin^2(\delta)]. \end{aligned} \quad (17)$$

As expected, this probability is larger than the value we would obtain for a uniform distribution in θ_2 , which is $\delta(\pi - \delta)/\pi^2$.

In general, to calculate the marginal distributions at the n 'th time the particle reaches the border, we have to integrate the joint distribution 13. For the incidence angle we obtain:

$$\begin{aligned} \rho_n(\gamma_n) &= \frac{\cos^2(\gamma_n)}{\pi^2} \int_{-\pi}^{\pi} \prod_{i=1}^{n-1} f(\theta_i, \delta) d\theta_i \\ &= \frac{\cos^2(\gamma_n)}{\pi^2} I_n(\gamma_n, \delta), \end{aligned} \quad (18)$$

while the expression for the marginal distribution in θ_n is:

$$\begin{aligned} \rho_n(\theta_n) &= \frac{1}{\pi^2} \int_{-\pi/2}^{\pi/2} \cos^2(\gamma_n) \prod_{i=1}^{n-1} f(\theta_i, \delta) d\gamma_n \\ &= \frac{1}{\pi^2} J_n(\theta_n, \delta). \end{aligned} \quad (19)$$

The distribution of the time t'_n may be found generalizing equation 16. The result is:

$$\rho_n(t'_n) = \frac{\tau_n^2 I_n(\gamma_n, \delta)}{(n-1)\pi^2 \sqrt{1 - \tau_n^2}}, \quad (20)$$

where $\tau_n = t'_n/(n-1)$ and $\cos(\gamma_n) = \tau_n$. It may be useful to stress that all probability distributions are normalized with respect to the initial condition, and thus the area under each marginal distribution is an decreasing function of n , since particles are leaving the vesicle at each time the border is reached.

To calculate of the integrals I_n and J_n defined above, we have to identify the region in the $(\theta_n, 2\gamma_n)$ plane where at least one of the f functions in the product vanish. The region where a particular function $f(\theta_{n-j}, \delta)$ vanishes is a set of $j+1$ parallel stripes, as may be seen in figure 2. In this figure, which corresponds to $n=4$, the two wider stripes correspond to $(\theta_4, 2\gamma_4)$ values such that $|\theta_3| < \delta$, the three stripes of intermediate width correspond to $|\theta_2| < \delta$ and points inside the four narrowest stripes are such that $|\theta_1| < \delta$. The expressions for the stripes are obtained by a recursive application of equations 11 which relate the variables at successive times the particle reaches the border.

The integrals I_n and J_n are continuous functions of their variables, but may display discontinuities in their derivatives. Their expressions are different in distinct ranges of their arguments. Although the calculation of

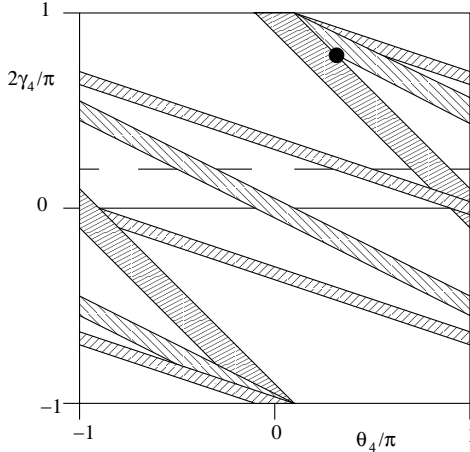


FIG. 2: Graphical representation of $\prod_{i=1}^{n-1} f(\theta_i, \delta)$, for $n = 4$ and $\delta = \pi/10$ as a function of θ_4 and γ_4 . The product vanishes in the shaded areas and is equal to one in the complement. The meanings of the circle and the horizontal segments at $\gamma_1 = \pi/10$ and $\gamma_1 = 0$ are explained in the text.

these functions is rather straightforward, the identification of the ranges of integration becomes harder as the number of the collision n grows, the number of different expressions increases quite fast with n . In the general case, we performed the calculations up to $n = 4$. For $\delta \geq \pi/2$, however, the calculation of the marginal distributions may be accomplished for any value of n . Some details of these calculations and the results are shown in the appendix.

Using the results for the marginal distribution ρ_3 we may obtain the probabilities:

$$p_3 = \frac{1}{2\pi^2} [\delta(2\pi - 3\delta) - 1 + 2\cos(\delta) - \cos(2\delta)], \quad \text{for } 0 \leq \delta \leq \frac{\pi}{2}; \quad (21)$$

$$p_3 = \frac{1}{2\pi^2} [\delta(\delta - 2\pi) + \pi^2 + 1 + \cos(2\delta) + 2\cos(\delta)], \quad \text{for } \frac{\pi}{2} \leq \delta \leq \pi. \quad (22)$$

The probability that the particle leaves the vesicle at its fourth arrival at the border is

$$p_4 = \frac{1}{6\pi^2} \left[\delta(6\pi - 13\delta) - 12 + 9\cos\left(\frac{2}{3}\delta\right) + 6\cos(\delta) - 3\cos(2\delta) \right], \quad \text{for } 0 \leq \delta \leq \frac{\pi}{3}; \quad (23)$$

$$p_4 = \frac{1}{6\pi^2} \left[\delta(5\delta - 6\pi) + 2\pi^2 - 3 + 9\cos\left(\frac{2}{3}\delta\right) - 6\cos(\delta) + 3\cos(2\delta) \right], \quad \text{for } \frac{\pi}{3} \leq \delta \leq \frac{\pi}{2}; \quad (24)$$

$$p_4 = \frac{1}{12\pi^2} \left[2\delta(\delta - 2\pi) + 2\pi^2 + 6 + 9\cos\left(\frac{2}{3}\delta\right) - 9\sqrt{3}\sin\left(\frac{2}{3}\delta\right) - 12\cos(\delta) \right], \quad \text{for } \frac{\pi}{2} \leq \delta \leq \pi. \quad (25)$$

Finally, using the marginal density for general $n \geq 2$

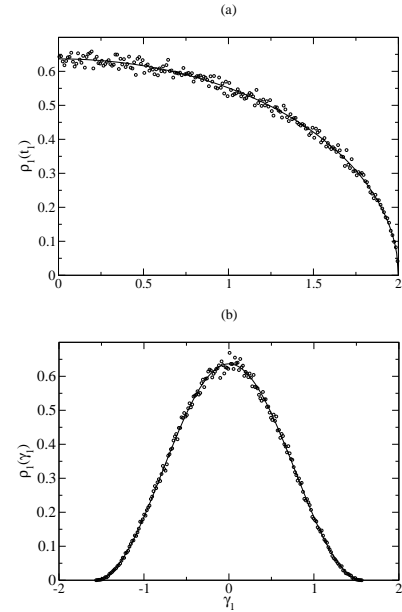


FIG. 3: Results from simulations for $\rho_1(t_1)$ (graph a) and $\rho_1(\gamma_1)$ (graph b). The numerical results are indicated by circles and the full lines are the corresponding analytical curves.

obtained for $\delta \geq \pi/2$ in the appendix, we obtain:

$$p_{n+1} = \frac{1}{2\pi^2 n(n-1)} \left[n(n-1) + 2\delta^2 + 2\pi(\pi - 2\delta) - n^2(n-1) \cos\left(\frac{(n-3)\pi + 2\delta}{n-1}\right) - n(n-1) \cos\left(\frac{2(\delta - \pi)}{n-1}\right) - n^2(n-1) \cos\left(\frac{2(\delta - \pi)}{n}\right) \right]. \quad (26)$$

III. DISCUSSION OF THE RESULTS AND COMPARISON WITH SIMULATIONS

Initially, we show results for $\rho_1(t_1)$ obtained with a simulation of 10^{11} particles starting at the initial condition, that is, initial position inside the unitary circle with uniform probability density and the direction of the initial velocity also uniformly distributed. In figure 3 the simulational results for the time of first arrival t_1 are shown and compared with the analytical expression (6). In the same figure the numerical results for $\rho_1(\gamma_1)$ are compared with expression (7). It is apparent that the numerical results are compatible with the analytical curves.

Although we realized many simulations starting from the initial condition, most of the numerical results shown here were obtained starting the simulation at the first collision of the particle with the wall ($n = 1$). With the same computational effort, these simulations led to

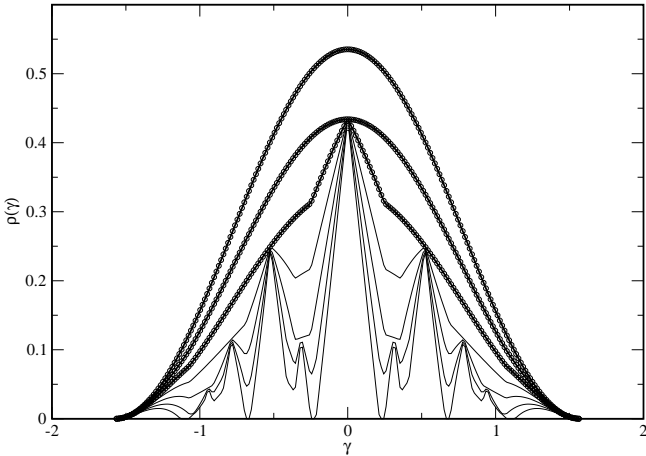


FIG. 4: Results for $\rho_n(\gamma_n)$ for $n = 2, 3, \dots, 8$. For the same value of γ , ρ_n is a non-increasing function of n . For $n = 2, 3, 4$ the numerical results are indicated by circles and the full lines are the corresponding analytical curves. For larger values of n , the lines correspond to results of simulations.

much better results than the ones starting from the initial condition, since only two variables define this condition now, instead of the three we have if the simulation starts at the initial condition. The numerical procedure followed in these simulations for a particular value of δ was:

1. N_θ of values for θ_1 , uniformly spaced in the interval $[-\pi, -\delta] \cup [\delta, \pi]$ are chosen.
2. For each value of θ_1 , N_γ values for the incidence angle γ_1 are generated randomly with the probability density 7 , and the subsequent loci of arrival of the particle are calculated for $n = 2, 3, \dots$, up to a maximum number n_{max} .
3. At the n 'th arrival at the border, the values of θ_n , γ_n , and t'_n are recorded, so that estimates for the marginal probability densities of these variables are obtained. If $-\delta \leq \theta_n \leq \delta$, the counter of the number of particles leaving the vesicle at the n 'th arrival at the border is increased by one and the simulation of a new particle starts. If $n = n_{max}$, the simulation of a new particle is started, otherwise we proceed to step $n + 1$.

The results shown below were obtained with the choices $N_\theta = 10^5$, $N_\gamma = 10^5$, so that a total of 10^{10} particles are considered in each simulation. We chose $n_{max} = 30$.

In figure 4 we show simulational and analytical results for the marginal distribution $\rho(\gamma)$ when $\delta = 0.5$. One notices that the agreement between simulation and theory is very good for the first four values of n , much better than the one observed in figure 3. This is due to the reduction of the number of initial conditions mentioned above. Another feature which is apparent in these data is that as n grows, peaks appear in the distribution at specific values of γ . The first peak to appear is located at $\gamma = 0$

and is already apparent in the analytical expression for $\rho_4(\gamma_4)$. These peaks are associated to periodic orbits in the vesicle, already discussed in [8]. Between two arrivals at the border, the angle θ changes as $\Delta\theta = \pi - 2\gamma$. If the orbit closes after p collisions and the particle performs q turns in the vesicle, we have $p\Delta\theta = 2\pi q$. Thus, the angle $\gamma_{p,q}$ for this periodic orbit is:

$$\gamma_{p,q} = \frac{p - 2q}{2p}\pi, \quad (27)$$

where p and q have no common divisors, $p \geq 2q$ and we considered only particles moving counterclockwise ($\Delta\theta > 0$). The periodic orbits may therefore be associated to the rational numbers q/p . For example, $p = 2, q = 1$, corresponds to $\gamma = 0$: the particle moves along a diameter. A polygonal orbit with p vertices corresponds to $(p, 1)$. A simple star with 5 vertices is described by $(5, 2)$.

In an open vesicle, only those periodic orbits with $\pi/p > \delta$ will last, and the peak will develop when $n > p$. The four peaks visible in figure 4 at non-vanishing γ may be identified as $(5, 2)$ ($\gamma = \pi/10$), $(3, 1)$ ($\gamma = \pi/6$), $(4, 1)$ ($\gamma = \pi/4$), and $(5, 1)$ ($\gamma = 3\pi/10$). The hexagon $(6, 1)$ still fulfills the condition above for the aperture $\delta = 0.5$ ($\pi/6 > 0.5$), but since it is quite close to the limit the corresponding peak at $\gamma_{6,1} = \pi/3$ is very small and hard to identify in the plots above. It is visible, however, in the results for larger values of n . Once a peak appears, it will narrow with increasing n . This may be explained noting that, of the particles with the corresponding angle $\gamma_{p,q}$, some will leave the vesicle, but only when $n \leq p$. Thus, the maximum value at the peak is stationary for $n > p$. However, particles with a slightly different incidence angle still leave the vesicle for $n > p$. As $n \rightarrow \infty$ the peak shrinks to just one point. The condition on the initial value of θ which assures that a particle with $\gamma = \gamma_{p,q}$ will never leave the vesicle is $\ell|\theta_1| > \delta$, for $\ell = 1, 2, \dots, p$ and reducing each angle to the interval $[-\pi, \pi]$. In summary, the periodic orbits correspond to horizontal segments in the (θ_1, γ_1) space of initial conditions. The initial conditions for a periodic orbit labeled as (q, p) in a vesicle with aperture δ are p segments at $\gamma_1 = \gamma_{p,q}$, with length $\Delta\Theta_1 = 2(\pi/p - \delta)$ and endpoints $|\theta_1|$ at $(\delta + 2\ell\pi/p, \delta + \ell\pi/p + \delta\theta)$, for $\ell = 0, 1, 2, \dots, p/2$. In figure 2 these segments were drawn for the star orbit $(5, 2)$ and for the diagonal orbit $(2, 1)$.

For $\delta > \pi/2$, all periodic orbits are suppressed, and we are able to calculate the marginal distribution for any n . In figure 5 results for $\delta = 1.6$ are shown for $n = 4, 5, 6$. The absence of peaks related to any periodic orbit is apparent, and for $n = 6$ the agreement between the analytical result (line) and the simulations (circles) may be appreciated. In this case, all particles with $|\gamma| < ((n+1)\delta - 2\pi)/(n-1)$ leave the vesicle at the n 'th time the border is reached or before.

Marginal distributions for θ are shown in figure 6 and compared with the analytical results for $n \leq 4$, also for the case $\delta = 0.5$. Again some peaks are observed, but

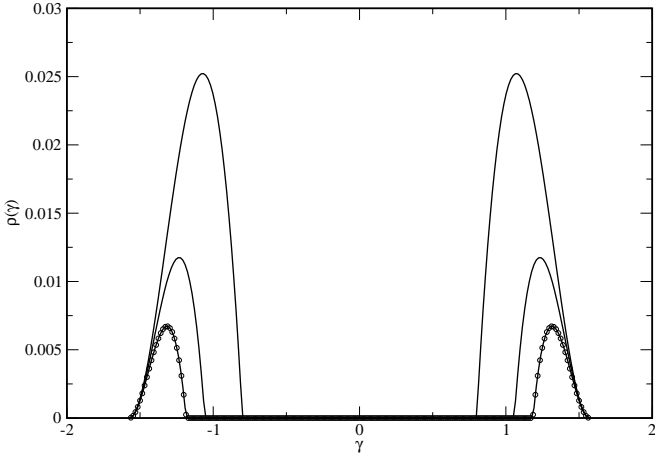


FIG. 5: Results for $\rho_n(\gamma_n)$ for $n = 4, 5, 6$ and $\delta = 1.6$. For $n = 6$ the numerical results are indicated by circles. Full lines are the analytical curves.

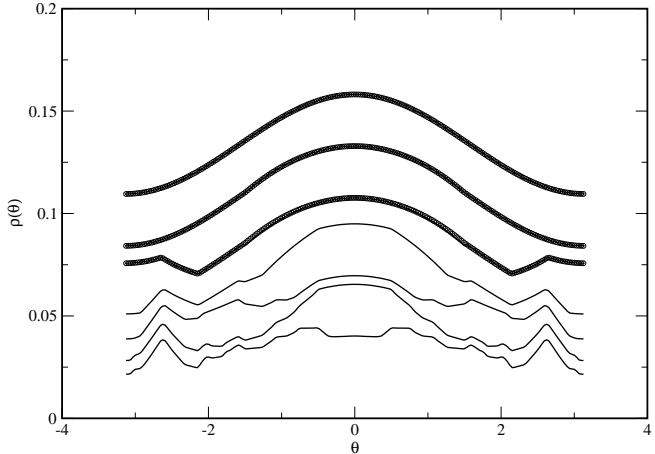


FIG. 6: Results for $\rho_n(\theta_n)$ for $n = 2, 3, 4 \dots 8$ and $\delta = 0.5$. For $n = 2, 3, 4$ the numerical results are indicated by circles and the full lines are the analytical curves. For $n > 4$, only simulational results are shown.

they are much broader than the ones in $\rho(\gamma)$. If we consider only a periodic orbit with p vertices, we would have p equally spaced rectangular peaks, of width $\Delta\theta_1$ defined above. Thus, as p grows approaching the limiting value π/δ the peaks become narrower. Therefore, for $\delta = 0.5$ the narrowest peaks belong to hexagons, and it is this peak we may identify for largest values of θ , located close to $\theta = 2.61$. For lower values of θ we have the superposition of several peaks and identification is harder. However, for larger n a step like structure develops at smaller θ , as expected. Although we do not show results here for $\delta > \pi/2$, where we obtained $\rho_n(\theta_n)$ analytically for any n , as expected smooth curves are found, since no periodic

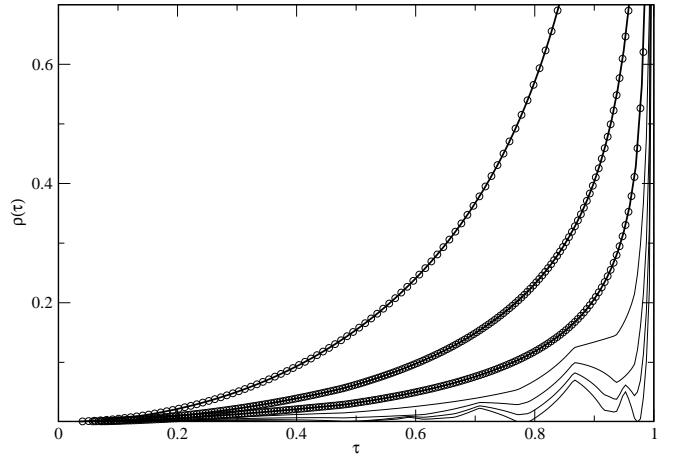


FIG. 7: Marginal density of probability of the time interval since the first arrival of the border, as a function of τ_n , for $n = 2, 3, \dots, 8$ and $\delta = 0.5$. Full lines for $n < 5$ correspond to analytical results and the circles are results from the simulations. For higher values of n only numerical results are presented.

orbits survive in this case. All particles with

$$|\theta| < \frac{(n+1)\delta - 2\pi}{n-1}$$

leave the vesicle at the n 'th arrival at the border or before.

In figure 7 we show results for the marginal distributions in the time t'_n between the n 'th and first arrival of the border. Again a good agreement between analytical and numerical results is found for $n = 2, 3, 4$. As expected, peaks develop at values which correspond to surviving periodic orbits, as may already be seen in the simulational results for larger values of n . The largest peak located at $\tau_n = t'_n/2(n-1) = 1$ corresponds to the diagonal periodic orbit $(2, 1)$, the other periodic orbits originate peaks at lower times. For $\delta > \pi/2$ again results for general n may be found and their agreement with simulational results is very good. Since just polygonal paths $q = 1$ survive after some collisions in this case, the maximum time a particle may spend inside the vesicle is $2(\pi - \delta)$. This result may be obtained from the general expression of $\rho_n(t'_n)$ in the limit $n \rightarrow \infty$.

Figure 8 shows results for the probability p_n that a particle leaves the vesicle as the border is reached the n 'th time, as a function of the aperture δ for the cases where analytic results are available. A good agreement is found between numerical and analytical results. In figure 9 we present numerical results for p_n as a function of n for some values of δ . We also included exponential functions which would be obtained for the escape probability if the distribution $\rho(\theta)$ would be always uniform, which are:

$$p_{n,u} = \left(1 - \frac{\delta}{\pi}\right)^{n-1} \frac{\delta}{\pi}. \quad (28)$$

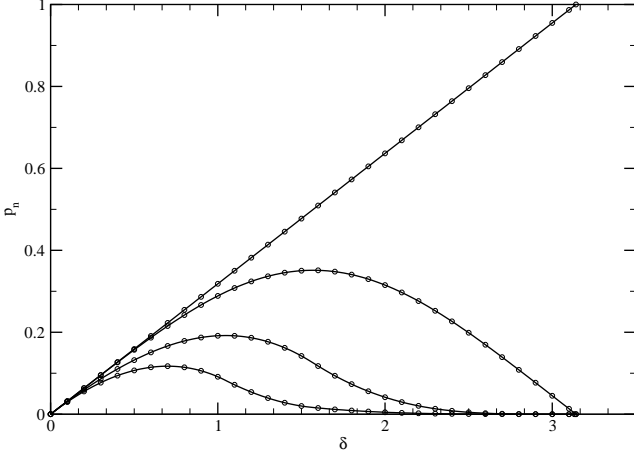


FIG. 8: Plots of p_n as a function of δ for $n = 1, 2, 3, 4$. Results from simulations are represented by circles and the lines are theoretical curves.

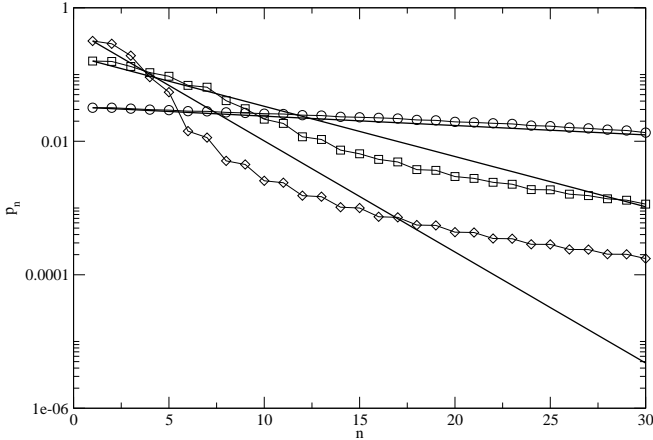


FIG. 9: Plots of p_n as a function of n for $\delta = 0.1$ (circles), $\delta = 0.5$ (squares), and $\delta = 1.0$ (diamonds). The thick lines are exponential functions discussed in the text.

First, we notice that the difference between the exponential decay and the results is lower for small values of δ . This may be explained recalling that for the closed circular billiard $\delta = 0$ the distribution $\rho(\theta)$ is uniform, so that, at least for small n , as δ increases the range of values of the probability density becomes larger. As mentioned above, p_2 is always larger than the value for an uniform distribution, but in general we observe that for an intermediate range of n , the exponential values are larger than the numerical results, but at sufficiently large n they again become smaller. For $\delta > \pi/2$, we may expand the expression 26 in $1/n$ and find the asymptotic power law behavior:

$$p_{n+1} = \pi^2(1 - \delta/\pi)^4 \left[\left(\frac{1}{n}\right)^4 + 2 \left(\frac{1}{n}\right)^5 - \dots \right], \quad (29)$$

so that in this case we may assure that p_n is larger than $p_{n,u}$ for sufficiently large values of n . It remains an open question if this conclusion extends to $\delta < \pi/2$, but our numerical results are consistent with this possibility. For $n = 3, 4$, p_n is larger than $p_{n,u}$ for δ in the range $]0, p_0[$ and smaller in the range $]p_0, \pi[$, where $p_0 = \pi/2$ for $n = 3$ and $p_0 = 0.919725\dots$ for $n = 4$.

IV. CONCLUSION

In our study of the open circular billiard, it is natural to obtain the distribution of the quantities of interest as a function of the collision number n . In other approaches, as usual, the time appears as the variable in terms of which the probability distributions are calculated. Although we did discuss somewhat the distribution of times at the first collisions, we did not enter in much detail in this question here. This is the subject of ongoing work. In the simulations, we also did not record results beyond 30 collisions with the wall, so that the question of the asymptotic decay of p_n for $\delta < \pi/2$ was not discussed in detail. As stated above, we have indications of a power law behavior, but the exponent may be different from the value 4 found exactly for larger apertures. One may imagine that the existence of orbits in which the particles are trapped forever inside the vesicle for $\delta < \pi/2$ may lead to a slower decay, with exponents smaller than 4 in this case. It is true, as may be seen above, that these orbits are a set of zero measure in the initial conditions, but particles in a finite region close to those orbits may take a long time to exit.

As was shown, the calculation of marginal distributions in the general case becomes more difficult for increasing n and finite $\delta < \pi/2$. There is, however, a simplification when $\delta \ll 1$, that is, if we consider the first terms in the expansion of the distributions in powers of δ . This is the range where other approaches, such as the one in [5], are effective.

There is a promising possibility to access the asymptotic behavior at long times if we recall that, after a certain number of collisions with the wall, the particles remaining in the vesicle will have incidence angles close to the values defined for the surviving periodical orbits. As another illustration of this, in figure 10 numerical results for the distribution of the time interval $t'_{20} = t_{20} - t_1$ are depicted in a logarithmic scale for a simulation with $\delta = 0.5$. The most important peak at $t'_{20} = 38$ corresponds to the vicinity of the diagonal orbit $(2, 1)$. The other peaks in order of decreasing values of t'_{20} are the same mentioned in the discussion of figure 4 above, but now the small peak corresponding to the hexagon $(6, 1)$ is visible centered at $t'_{20} = 38 \cos(\gamma_{6,1}) = 38 \cos(\pi/3) = 19$. The small continuous distribution at low times corresponds to particles in high p orbits, which still did not reach the aperture after 19 collisions. As discussed above, this distribution is located at times smaller than $2(\pi - \delta)$ and does not contribute at larger times. We are presently

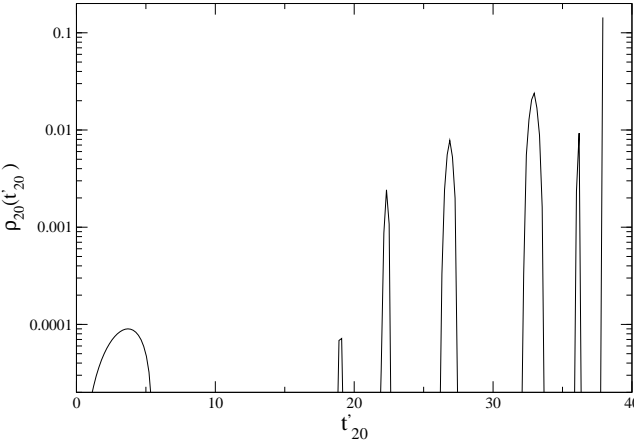


FIG. 10: Probability density of the time interval t'_20 obtained from simulations with $\delta = 0.5$. The peaks which correspond to the neighborhood of surviving periodic orbits are apparent.

working on an approach where the neighborhood of the periodic orbits is treated in a approximate way, which is should be appropriate for the discussion of the long time limit.

Acknowledgements

We thank Prof. Ronald Dickman for having brought reference [5] to our attention and Profs. Yan Levin, Marco Idiart, and Domingos U. Marchetti for helpful discussions. This work was partially financed by project Pronex-CNPq-FAPERJ/171.168-2003.

APPENDIX A: CALCULATION OF I_n AND J_n

Both $I_n(\gamma_n, \delta)$ and $J_n(\theta_n, \delta)$ are even functions of their first argument, so we restrict the calculations below to non-negative values of these variables. As may be seen in figure 2, the domains of integration are split into regions where the product of f functions is equal to unity. This regions change as the variables of the marginal distributions are varied, so that these distributions are given by different expression in different areas of the domain of their arguments. It is convenient to use the variable $\phi_n = 2\gamma_n$ in the functions I_n . For I_3 these areas are shown in figure 11.

For a particular value of the argument ϕ_3 , I_3 is equal to the sum of the segments in white regions of the corresponding horizontal line in figure 2, if we erase the narrowest stripes which correspond to $n = 4$. For $\delta \leq \pi/2$, this total length is equal to $2\pi - 4\delta$ if $\phi_3 \leq \pi - 2\delta$ and to $\pi + \phi_3 - 2\delta$ otherwise. In general, the expressions

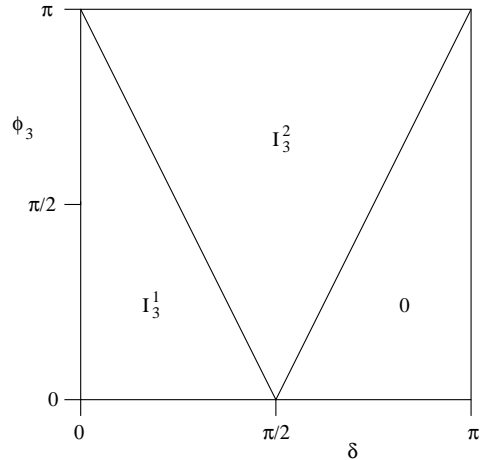


FIG. 11: Regions of the domain of the arguments where $I_3(\gamma_n, \delta)$ is given by different expressions. The function I_3 vanishes in the triangular region labeled by 0.

for I_3 in the triangular regions depicted in figure 3 are

$$I_3^1 = 2\pi - 4\delta, \quad (A1)$$

$$I_3^2 = \pi + \phi_3 - 2\delta. \quad (A2)$$

In these calculations, the crossings of the borders of the stripes determine the limits of the region in the arguments where each expression is valid. These borders have the general form

$$\theta_{n+1} + n\phi_{n+1} = (n - 2\ell)\pi \pm \delta, \quad (A3)$$

where the plus sign is for the upper border and the minus sign for the lower border of the stripe and $0 \leq \ell \leq n$ labels the stripes in each order n . As an example of such a crossing of borders, we have the point indicated by a circle in figure 2, which corresponds to the crossing of the lines ($n = 3, \ell = 0, -$) and ($n = 2, \ell = 0, +$) and is located at $\theta = 3\delta, \phi = \pi - 2\delta$.

For the calculation of J_n , each vertical segment in the white region of the diagram 2, limited by ϕ_- and ϕ_+ contributes with $g(\phi_+) - g(\phi_-)$ to the function J_n , where integrating equation (19) we get:

$$g(\phi) = \frac{1}{4}[\phi + \sin(\phi)]. \quad (A4)$$

We may then obtain the expressions for J_3 . The diagram indicating the region where each expression is valid is shown in the figure 12. The expressions are:

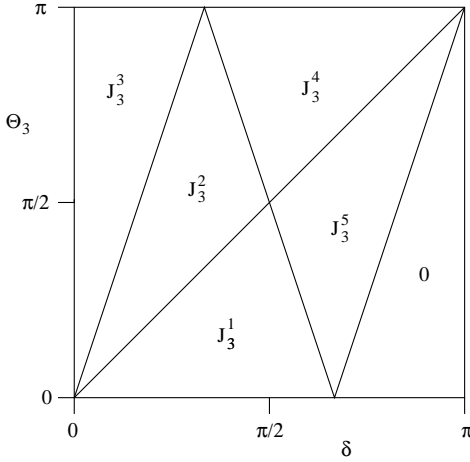


FIG. 12: Regions of the domain of the arguments where $J_3(\gamma_3, \delta)$ is given by different expressions. The equations of the limiting lines are $\theta_3 = \delta$, $\theta_3 = 3\delta$, $\theta_3 = 2\pi - 3\delta$, and $\theta_3 = \delta - 2\pi$. J_3 vanishes in the region labeled by 0.

$$J_3^1 = \frac{1}{2} \left[\pi - \frac{3}{2}\delta - \cos(\theta_3/2) \sin(\delta/2) + \cos(\theta_3) \sin(\delta) \right], \quad (\text{A5})$$

$$J_3^2 = \frac{1}{2} \left[\pi - \frac{\theta_3}{4} - \frac{5}{4}\delta + \frac{1}{2} \sin(\theta_3 + \delta) - \frac{1}{2} \sin\left(\frac{\theta_3 + \delta}{2}\right) \right], \quad (\text{A6})$$

$$J_3^3 = \frac{\pi}{2} - \delta + \frac{1}{2} \cos(\theta_3) \sin(\delta), \quad (\text{A7})$$

$$J_3^4 = \frac{1}{2} \left[\frac{\pi}{2} - \frac{\delta}{2} - \sin\left(\frac{\theta_3}{2}\right) \cos\left(\frac{\delta}{2}\right) \right], \quad (\text{A8})$$

$$J_3^5 = \frac{1}{4} \left[\pi + \frac{\theta_3}{2} - \frac{3}{2}\delta - \sin(\theta_3 - \delta) - \sin\left(\frac{\theta_3 + \delta}{2}\right) \right]. \quad (\text{A9})$$

For $n = 4$, the function $I_4(\gamma_4, \delta)$ is given by three different expressions in the triangular regions indicated in figure 13, vanishing in the fourth region in the space of its arguments. The expressions are:

$$I_4^1 = 2(\pi - \phi_4 - 2\delta) \quad (\text{A10})$$

$$I_4^2 = 2(\pi - 3\delta) \quad (\text{A11})$$

$$I_4^3 = 2(\phi_4 - \delta). \quad (\text{A12})$$

Finally, in figure 14 the domain of the arguments of the function $J_4(\theta_4, \delta)$ is depicted, with a total of 18 regions where different expressions are valid. The expressions

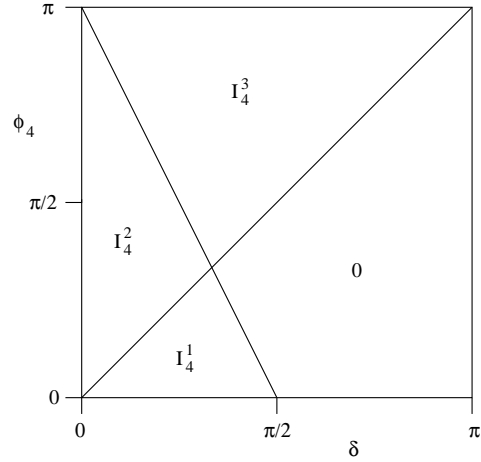


FIG. 13: Regions of the domain of the arguments where $I_4(\phi_4, \delta)$ is given by different expressions. The equations of the limiting lines are $\phi_4 = \delta$ and $\phi_4 = \pi - 2\delta$. I_4 vanishes in the region labeled by 0.

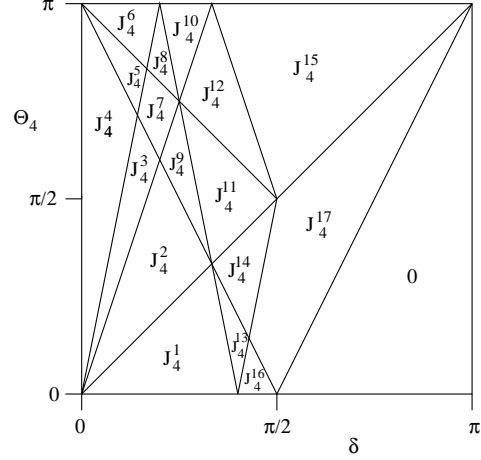


FIG. 14: Regions of the domain of the arguments where $J_4(\theta_4, \delta)$ is given by different expressions. The equations of the limiting lines are $\theta_4 = \delta$, $\theta_4 = 3\delta$, $\theta_4 = 5\delta$, $\theta_4 = 2\pi - 5\delta$, $\theta_4 = \pi - 2\delta$, $\theta_4 = \pi - \delta$, $\theta_4 = 2\pi - 3\delta$, $\theta_4 = -\pi + 2\delta$, and $\theta_4 = 5\delta - 2\pi$. J_4 vanishes in the region labeled by 0.

are:

$$J_4^1 = \frac{1}{2} \left[\pi - \frac{13}{6}\delta + \cos(\theta_4) \sin(\delta) - \cos\left(\frac{\theta_4}{3}\right) \sin\left(\frac{\delta}{3}\right) - \cos\left(\frac{\theta_4}{2}\right) - \sin\left(\frac{\delta}{2}\right) \right], \quad (\text{A13})$$

$$J_4^2 = \frac{1}{2} \left[\pi - \frac{\theta_4}{3} - \frac{11}{6}\delta + \frac{1}{2} \sin(\theta_4 + \delta) - \frac{1}{2} \sin\left(\frac{\theta_4 + \delta}{3}\right) - \cos\left(\frac{\theta_4}{2}\right) \sin\left(\frac{\delta}{2}\right) \right], \quad (\text{A14})$$

$$J_4^3 = \frac{1}{2} \left[\pi - \frac{\theta_4}{12} - \frac{31}{12} \delta + \cos(\theta_4) \sin(\delta) - \frac{1}{2} \sin\left(\frac{\theta_4 + \delta}{3}\right) + \frac{1}{2} \sin\left(\frac{\theta_4 - \delta}{2}\right) \right], \quad (\text{A15})$$

$$J_4^4 = \frac{1}{2} [\pi - 3\delta + \cos(\theta_4) \sin(\delta)], \quad (\text{A16})$$

$$J_4^5 = \frac{\pi}{3} + \frac{\theta_4}{6} - \frac{7}{6} \delta - \frac{1}{4} \sin(\theta_4 - \delta) + \frac{\sqrt{3}}{8} \cos\left(\frac{\theta_4 - \delta}{3}\right) - \frac{1}{8} \sin\left(\frac{\theta_4 - \delta}{3}\right), \quad (\text{A17})$$

$$J_4^6 = \frac{\pi}{2} - \frac{4}{3} \delta + \frac{1}{2} \cos(\theta_4) \sin(\delta) + \frac{\sqrt{3}}{4} \sin\left(\frac{\theta_4}{3}\right) \sin\left(\frac{\delta}{3}\right) + \frac{1}{4} \cos\left(\frac{\theta_4}{3}\right) \sin\left(\frac{\delta}{3}\right), \quad (\text{A18})$$

$$J_4^7 = \frac{\pi}{3} + \frac{\theta_4}{8} - \frac{23}{24} \delta + \frac{\sqrt{3}}{8} \cos\left(\frac{\theta_4 - \delta}{3}\right) - \frac{1}{4} \sin\left(\frac{\theta_4 + \delta}{3}\right) - \frac{1}{8} \sin\left(\frac{\theta_4 - \delta}{3}\right) + \frac{1}{4} \sin\left(\frac{\theta_4 - \delta}{2}\right) - \frac{1}{4} \sin(\theta_4 - \delta), \quad (\text{A19})$$

$$J_4^8 = \frac{1}{2} \left[\pi - \frac{\theta_4}{12} - \frac{9}{4} \delta + \cos(\theta_4) \sin(\delta) - \frac{1}{2} \sin\left(\frac{\theta_4}{3}\right) \cos\left(\frac{\delta}{3}\right) + \frac{\sqrt{3}}{2} \sin\left(\frac{\theta_4}{3}\right) \sin\left(\frac{\delta}{3}\right) + \frac{1}{2} \sin\left(\frac{\theta_4 - \delta}{2}\right) \right], \quad (\text{A21})$$

$$J_4^9 = \frac{\pi}{3} + \frac{7}{12} \delta + \frac{\sqrt{3}}{8} \cos\left(\frac{\theta_4 - \delta}{3}\right) - \frac{1}{4} \sin\left(\frac{\theta_4 + \delta}{3}\right) - \frac{1}{8} \sin\left(\frac{\theta_4 - \delta}{3}\right) - \frac{1}{2} \cos\left(\frac{\theta_4}{2}\right) \sin\left(\frac{\delta}{2}\right), \quad (\text{A22})$$

$$J_4^{10} = \frac{1}{2} \left[\frac{5}{6} \pi + \frac{11}{6} \delta - \frac{1}{2} \sin\left(\frac{\pi + \theta_4 + \delta}{3}\right) + \sin\left(\frac{\theta_4}{2}\right) \cos\left(\frac{\delta}{2}\right) + \cos(\theta_4) \sin(\delta) - \frac{1}{2} \sin\left(\frac{\theta_4 - \delta}{3}\right) \right], \quad (\text{A23})$$

$$J_4^{11} = \frac{1}{2} \left[\frac{\pi}{2} + \frac{\theta_4}{12} - \frac{3}{4} \delta - \sin\left(\frac{\theta_4}{3}\right) \cos\left(\frac{\delta}{3}\right) + \frac{1}{2} \sin\left(\frac{\theta_4 - \delta}{2}\right) \right], \quad (\text{A24})$$

$$J_4^{12} = \frac{1}{4} \left[\frac{5}{3} \pi + \frac{\theta_4}{2} - \frac{13}{6} \delta - \sin\left(\frac{\pi + \theta_4 + \delta}{3}\right) + \sin\left(\frac{\theta_4 - \delta}{2}\right) - \sin\left(\frac{\theta_4 - \delta}{3}\right) + \sin(\theta_4 + \delta) \right], \quad (\text{A25})$$

$$J_4^{13} = \frac{1}{2} \left[\frac{5}{6} \pi + \frac{1}{12} \theta_4 - \frac{7}{4} \delta + \cos(\theta_4) \sin(\delta) - \frac{1}{2} \sin\left(\frac{\pi + \theta_4 + \delta}{3}\right) + \frac{1}{2} \sin\left(\frac{\theta_4 - \delta}{2}\right) - \sin\left(\frac{\theta_4 + 2\delta}{6}\right) \sin\left(\frac{\delta}{3}\right) \right], \quad (\text{A26})$$

$$J_4^{14} = \frac{1}{4} \left[\pi + \frac{5}{6} \theta_4 - \frac{16}{6} \delta - \sin(\theta_4 - \delta) - \sin\left(\frac{\pi + \theta_4 + \delta}{3}\right) + \sin\left(\frac{\theta_4 - \delta}{2}\right) + \cos\left(\frac{\pi + 2\theta_4 + 2\delta}{6}\right) \right], \quad (\text{A27})$$

$$J_4^{15} = \frac{1}{2} \left[\frac{\pi}{3} - \frac{\delta}{3} - \frac{1}{2} \sin\left(\frac{\pi + \theta_4 + \delta}{3}\right) - \frac{1}{2} \sin\left(\frac{\theta_4 - \delta}{3}\right) \right], \quad (\text{A28})$$

$$J_4^{16} = \frac{\pi}{3} - \frac{2}{3} \delta + \frac{1}{2} \cos(\theta_4) \sin(\delta) - \frac{\sqrt{3}}{4} \cos\left(\frac{\theta_4}{3}\right) \cos\left(\frac{\delta}{3}\right) - \frac{1}{4} \cos\left(\frac{\theta_4}{3}\right) \sin\left(\frac{\delta}{3}\right), \quad (\text{A29})$$

$$J_4^{17} = \frac{\pi}{6} + \frac{\theta_4}{6} - \frac{\delta}{3} - \frac{1}{4} \sin(\theta_4 - \delta) - \frac{1}{4} \sin\left(\frac{\pi + \theta_4 + \delta}{3}\right). \quad (\text{A30})$$

The extension of these calculations to larger values of n becomes increasingly difficult and will not be presented here. However, for $n \geq 2$ and $\delta \geq \pi/2$ a major simplification occurs and it is easy to perform the calculations of I_{n+1} and J_{n+1} , since in the diagram corresponding to figure 2 in this case the white area is reduced to only two triangles and two quadrangles. The vertices of the first triangle are located at $\theta = \phi = -\pi$, $\theta = -\pi, \phi = -\pi(1 - 1/n)$, and $\theta = -\delta, \phi = -\pi$. The second triangle may be obtained by transforming $\theta \rightarrow -\theta$ and $\phi \rightarrow -\phi$. The vertices of the quadrangle are located at $\theta = \pi, \phi = -\pi$, $\theta = \pi, \phi = -\pi(1 - 1/n)$, $\theta = \delta, \phi = -\pi$, and $\theta = (\delta(n+1) - 2\pi)/(n-1), \phi = -((n-3)\pi + 2\delta)/(n-1)$. The second quadrangle may be obtained by the same projection operation described above. We then obtain

$$I_{n+1} = 0, \text{ for } 0 \leq \phi_{n+1} \leq \frac{(n-3)\pi + 2\delta}{n-1}; \quad (\text{A31})$$

$$I_{n+1} = (3-n)\pi - 2\delta + (n-1)\phi_{n+1}, \quad \text{otherwise.} \quad (\text{A32})$$

For the function related to the marginal distribution in θ_{n+1} we get the result $J_{n+1} = 0$ for $0 \leq \theta_{n+1} \leq$

$((n+1)\delta - 2\pi)/(n-1)$ and:

$$J_{n+1} = \frac{1}{4} \left[\frac{2\pi - \theta_{n+1} - \delta}{n} + \theta_{n+1} - \delta - \sin \left(\frac{(n-2)\pi + \theta_{n+1} = \delta}{n} \right) - \sin(\theta_{n+1} - \delta) \right],$$

for $\frac{(n+1)\delta - 2\pi}{n-1} \leq \theta_{n+1} \leq \delta$; (A33)

$$J_{n+1} = \frac{1}{4} \left[\frac{2}{n} (\pi - \theta_{n+1}) - \sin \left(\frac{(n-2)\pi + \theta_{n+1} + \delta}{n} \right) - \sin \left(\frac{\theta_{n+1}}{n} \right) \right], \text{ for } \delta \leq \theta_{n+1} \leq \pi. \quad (A34)$$

- [1] W. Bauer and G. F. Bertsch, Phys. Rev. Lett. **65**, 2213 (1990).
- [2] O. Legrand and D. Sornette, Europhys. Lett. **11**, 583 (1990); Phys. Rev. Lett. **66**, 2172 (1991).
- [3] W. Bauer and G. F. Bertsch, Phys. Rev. Lett. **66**, 2173 (1991).
- [4] H. Alt et al, Phys. Rev E **53**, 2217 (1996).
- [5] E. Vicentini and V. B. Kokshenev, Physica A **295**, 391 (2001).
- [6] Ya. G. Sinai, Russ. Math. Surveys **25**, 137 (1970).
- [7] L. A. Bunimovich, Funct. Anal. Appl. **8**, 254 (1974); Commun. Math. Phys. **65**, 295 (1979); Zh. Eksp. Teor. Fiz. **89**, 1452 (1985) [Sov. Phys. JETP **62**, 842 (1985)].
- [8] S. Ree and L. E. Reichl, Phys. Rev E **60**, 1607 (1999).